INTEGRATED THERMAL HYDRAULIC ANALYSIS OF HOT AND COLD POOLS OF A LIQUID SODIUM COOLED 600 MWE FAST REACTOR

Ram Kumar Maity, M. Rajendrakumar, K. Natesan, S. Raghupathy

Indira Gandhi Centre for Atomic Research, Kalpakkam, India

Email contact of corresponding author: rammaity@igcar.gov.in

Abstract

Hot and cold pools along with immersed components represent the primary heat transport system of a pool type fast reactor. The two pools are physically separated by inner vessel, which completely envelopes the hot pool. Cold pool along with inner vessel is enveloped by main vessel. Inner vessel is in contact with both hot and cold pools, having widely different temperatures. Apart from this, the complex flow patterns in hot and cold pools introduce circumferential and axial temperature asymmetry on both inner and main vessels. The combination of complex computational domain and flow physics necessitates a detailed three dimensional CFD study. Towards this, a three dimensional CFD model that includes both hot and cold pools along with all major immersed components is developed. Development of a three dimensional model is a challenging task due to the large dimensions, several immersed solid structures and requirement of modelling components with widely different scales. The main focus of the present work is on resolution of temperature distributions of important structural components, viz., inner vessel, main vessel, primary piping, pump and heat exchanger standpipes, headers etc. during full power operating conditions of reactor. Heat bypass from hot to cold pool through inner vessel is another important quantity estimated from this study.

1. INTRODUCTION

The present study is on a proposed two loop 600 MWe pool type fast reactor design. As part of studies towards optimisation of design aspects, a comprehensive CFD model of reactor pool and immersed components is developed for detailed thermal hydraulic studies. Hot and cold pools along with immersed components represent the primary heat transport (PHT) system. Fig. 1 shows the vertical section and top view of reactor assembly of FBR1&2. Nuclear heat generated in reactor core is carried by liquid sodium coolant into the hot pool. From hot pool, hot sodium further enters four intermediate heat exchangers (IHX) where secondary sodium carries heat to steam generators through secondary heat transport system. Primary sodium after cooling down in IHX flows into cold pool. From here, cold sodium is pumped by 3 Primary Sodium Pumps (PSP) into Grid Plate (GP) from where it enters the reactor core. Sodium inside grid plate has two additional leakage paths. Leakage from top enters hot pool through inter-wrapper space. Leakage from bottom of grid plate feeds into the main vessel cooling system and drains into cold pool.

Hot and cold pools are physically separated by Inner Vessel (IV), which completely envelopes the hot pool. Cold pool along with inner vessel is enveloped by Main Vessel (MV). Thus, inner vessel is in contact with both hot and cold pools, having widely different temperatures. Apart from this, the complex flow patterns in hot and cold pools introduce circumferential and axial temperature asymmetry on both inner vessel and main vessel. The main focus of this work is on resolving temperature distributions of important structural components, viz., inner vessel, main vessel, primary piping, primary pump standpipes, spherical headers etc. during full power operating conditions of reactor. Apart from structural temperatures, heat transfer from hot to cold pool through inner vessel is another important quantity estimated from this study. This heat bypass has repercussions for plant efficiency. The combination of complex flow physics necessitates a detailed three dimensional CFD study. Towards this, a three dimensional CFD model that includes both hot and cold pools along with all major immersed components is developed.

Earlier axi-symmetric studies of Reactor pool were utilised to estimate inner vessel temperature distribution along with heat transfer from hot pool to cold pool [1]. These studies were computationally less expensive and took advantage of the axi-symmetric nature of reactor assembly at specific circumferential positions. However, these studies were incapable of resolving the effect of various components passing through

Reactor assembly cross section

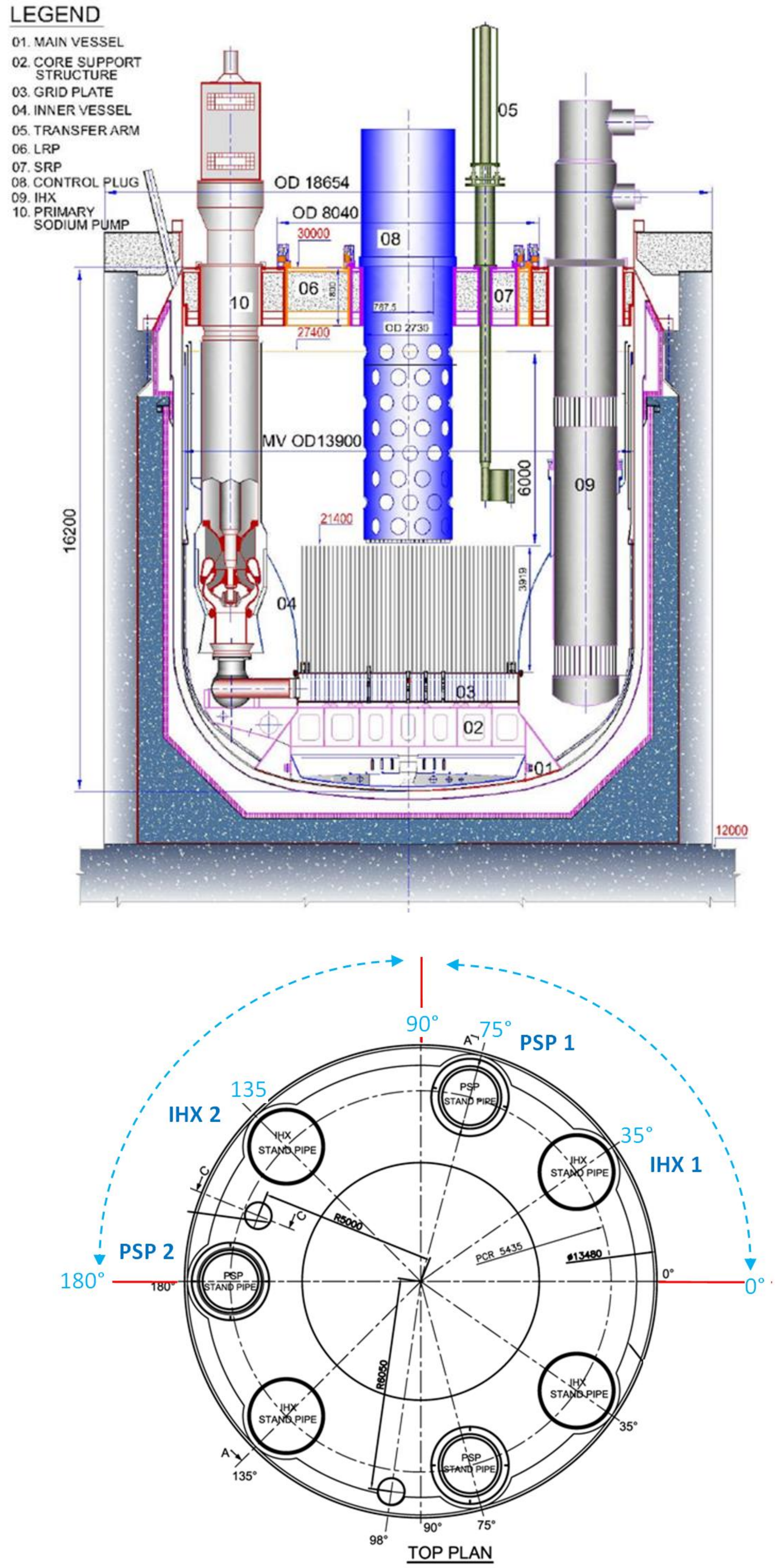

FIG. 1: Cross Sectional and top views of reactor assembly

the inner vessel, viz., IHX and PSP. Also, the effect of immersed components on flow field also could not be accounted. Therefore, even though a reasonable estimate of axial distribution of temperature of inner vessel valid for limited circumferential positions was estimated, circumferential variation was unavailable. The present study allows comprehensive prediction of pool temperature and flow fields.

2. COMPUTATIONAL MODEL

Development of a three dimensional model is a challenging task due to the large dimensions, several immersed solid structures and requirement of modelling components with widely different scales. For example, the diameter at top of inner vessel is about 13.5 m with its thickness being about ~15 mm. Further inclusion of internal structures like spherical headers, Primary piping etc. complicates the task of mesh generation. The model developed for the present study is a 180º sector model to take advantage of inherent symmetry. The sector modelled is shown in Fig. 1 along with the convention followed to mark angular positions. The complete CFD model is modelled using hexahedral cells. However, mesh interfaces along with non-conformal grids are employed and also ensuring interfaces are limited.

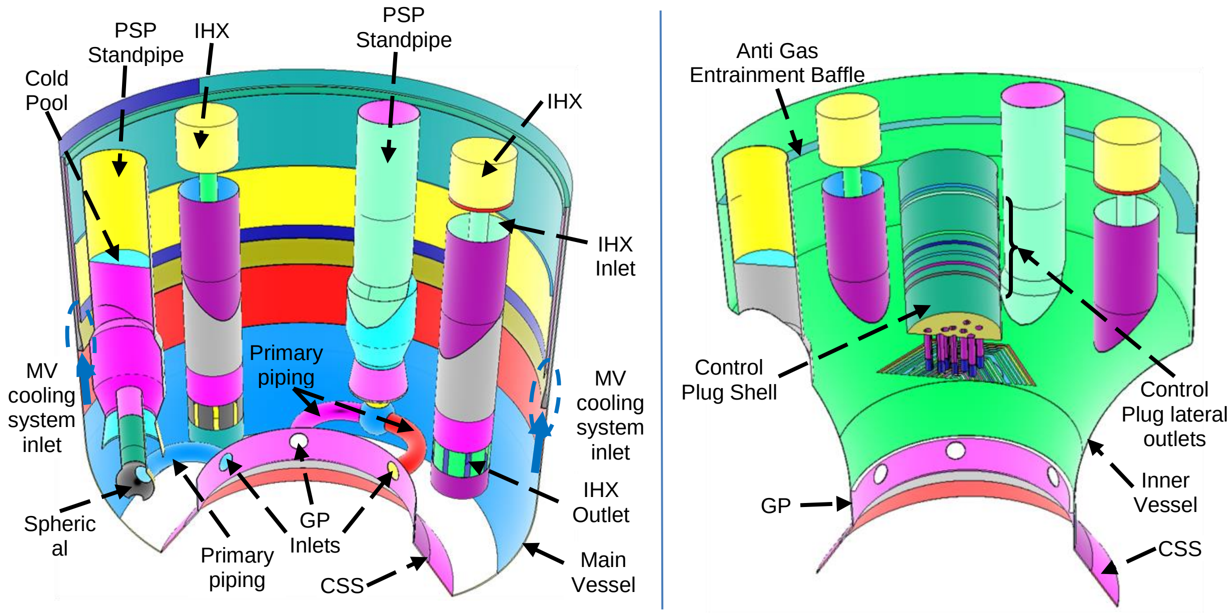

FIG. 2: Depiction of important modelled internal (immersed) structures of cold and hot pools with some important boundaries

Internal details of the model developed for the present study are shown in Figs. 2 & 3. Important structures immersed in main vessel, viz., PSP standpipes, IHX standpipes, spherical headers, primary piping etc. are shown in Fig. 2. All these structures are modelled as solids with material of construction being SS 316 LN. The outlet for the model is at GP inlets. IHX outlet can also be seen here where; multiple equally spaced vertical impervious baffles are placed to account for the flow area blocked by IHX tubes at its outlet. This captures the reduction in flow area and the resulting increase in outlet velocity due to the presence of IHX tubes. In the same figure, main vessel cooling system is also shown, which is modelled starting from main vessel cooling system inlet. Sodium at 670 K from bottom leakage of grid plate is fed into the main vessel cooling system. This is modelled with velocity inlet boundary condition.

Fig. 3 shows the intricate details of the region above core top. The upper boundary of this domain is represented by an impervious Core Cover Plate (CCP) modelled as non-slip adiabatic wall. Sodium flows into control plug through control rod shrouds as shown. These shrouds are also modelled as non-slip adiabatic walls and admit a small percentage of total core flow. This is implemented using a mass sink boundary specified at the bottom base of shroud tubes. The main sodium inlet to hot pool is from core outlet which is modelled as a set of concentric hexagonal rings. Discrete subassembly outlets are clumped into hexagonal rings such that flow area of each ring is exactly equal to the sum of outlet areas of subassemblies in that hexagonal row in the core. More details are available in ref. [2 - 4]. The region between hexagonal rows is divided between impermeable and permeable regions. These permeable regions act as connections between hot pool and SA inter-wrapper space and allow sodium to enter from hot pool (below CCP) into inter-wrapper space. The area of permeable regions is equal to the area of inter-wrapper gap.

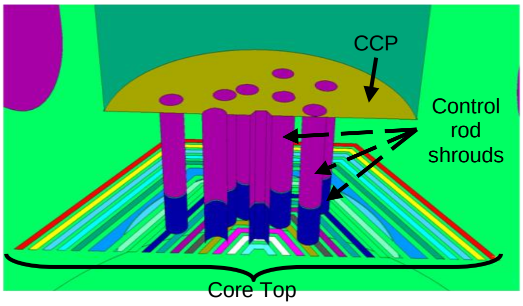

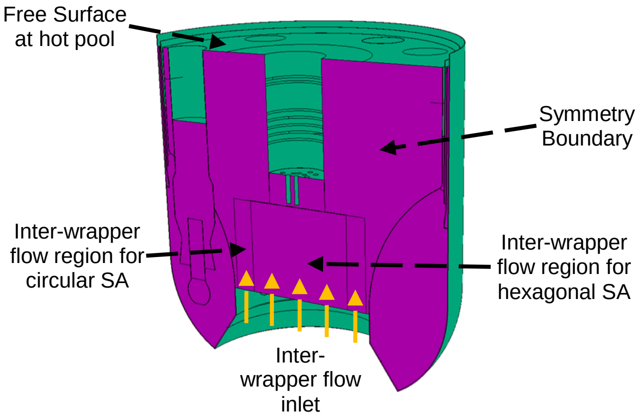

FIG. 3: Modelling approach for important boundaries

Lattice plate and porous skirt (shown in Fig. 5) are modelled as porous jump boundaries with pressure drop coefficient for flow in normal direction being calculated based on Ward Smith's correlation [5]. Pressure drop in normal direction is given by: $\Delta P_n = k\frac{1}{2}\rho V_n{}^2$, where the subscript 'n' stands for normal direction. Figure 2 also shows the structures bounding the hot pool, viz., Inner Vessel, Grid Plate (GP) and Core Support Structure (CSS). These structures are also modelled as solid structures similar to other structures. The inner surfaces of GP and CSS are modelled as isothermal walls maintained at cold pool temperature. Inner vessel provides thermal connection between hot and cold pools through which conjugate heat transfer takes place. Sodium from hot pool that enters shroud tubes, exits control plug and re-enters hot pool through seven rows of holes on lateral shell of control plug. These are modelled as circumferential strips on lateral wall of control plug. The temperature of sodium exiting control plug lateral shell is taken to be equal to the mass weighted average temperature of sodium entering control rod shrouds.

Figure 3 displays some more important modelling details. All fluid (free) surfaces, both in hot and cold pools are modelled as free slip walls. Symmetry boundary for the 180° symmetry model is also shown here. For inter-wrapper region, an inlet at the bottom (as shown in Fig. 7) is provided to account for top leakage flow from grid plate. The inter-wrapper region itself is modelled as a porous zone. In order to account for the pressure drop offered by subassemblies, anisotropic three dimensional pressure drop coefficients are imposed on the porous zone. Two different zones representing central hexagonal subassemblies and peripheral circular/shielding subassemblies are modelled. Each zone has a different pressure drop correlation. A similar approach is followed for capturing effect of tube bundle in IHX on flow field. Pressure drop offered by porous zone(s) in x, y and z-directions are calculated using the following correlations [6]:

For pressure drop in transverse directions (x, y):

For a=1.25 and 3 < Re < 103, $\frac{Eu}{k_1} = 0.795 + \frac{0.247e3}{Re} + \frac{0.335e3}{Re^2} - \frac{0.155e4}{Re^3} + \frac{0.241e4}{Re^4}$

For a=1.25 and 103< Re < 106, $\frac{Eu}{k_1} = 0.245 + \frac{0.339e4}{Re} - \frac{0.984e7}{Re^2} + \frac{0.132e11}{Re^3} - \frac{0.599e13}{Re^4}$

Where, *Re* stands for Reynold's number, *Eu* stands for Euler's number, k_1 equals 1 for an equilateral triangular array, a is the ratio of lateral pitch to tube diameter

Pressure drop is calculated from Euler's number: $\Delta P = Eu\frac{\rho u^2}{2}z$

Where, *z* is the number of tube rows, *u* is the Superficial velocity (m/s).

For pressure drop in axial direction: $\Delta P = \left(f\,\frac{L}{D}\right)\frac{\rho u^2}{2}$

Where, f = 64/Re (laminar) or 0.316/$Re^{0.25}$ (turbulent flow), L= Length of tube bundle in m and D is Hydraulic diameter of tube bundle, m.

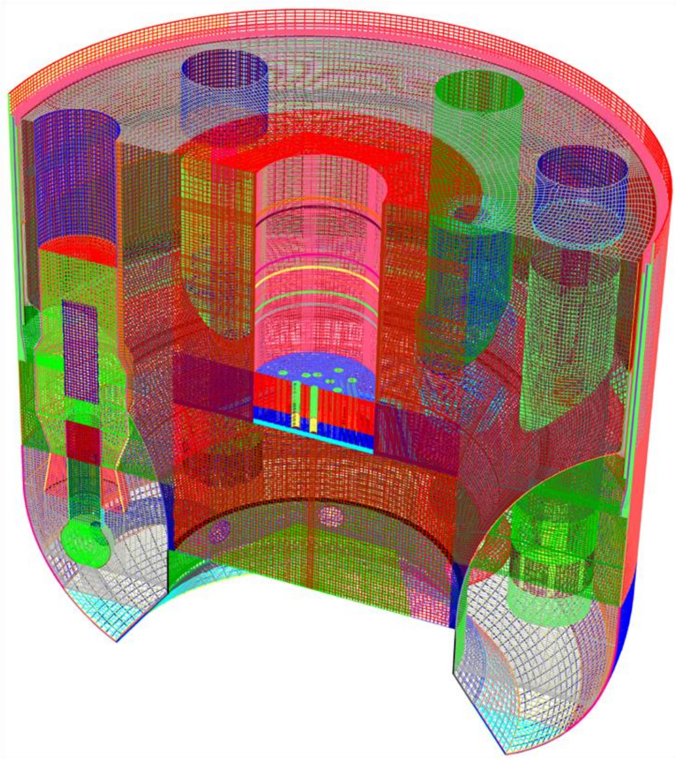

FIG. 4: Mesh developed for analysis

The equations of conservation for mass, momentum and energy similar to those discussed in [7] are discretised and solved first to derive a steady state flow and temperature field. Heat transfer from primary to secondary heat transport system in IHX is simulated by imposing a uniform heat sink on the IHX volume. The final mesh developed is shown in Fig. 4. Hexahedral elements are used exclusively in combination with mesh interfaces. Mesh interfaces are used to connect parts of the model meshed separately to ensure connectivity. The total number of elements used is about 2.6 million (including both fluid and solid volumes). Effects of turbulence are modelled using the κ-ε high Reynolds (realizable) model [8]. SIMPLE algorithm is used to allow pressure velocity coupling. First order UPWIND schemes are used to discretize conservation equations of momentum, turbulence quantities and species concentration. A pressure staggering option (PRESTO) is used to discretize the continuity equation. To declare convergence, it was ensured that all residues are ~ 10-6. Conservation equation of mass, momentum and energy are solved using Fluent Ver.19.2 [8].

3. RESULTS AND DISCUSSION

3.1. Velocity and Temperature

Velocity vectors at the symmetry plane are shown in Fig. 5. This section bisects PSP 2 and gives an overview of velocity pattern of fluid flow in both hot and cold pools. On expected lines, sodium exiting axially from core outlet meets the core cover plate at the top and is forced to turn and attain a dominant radial component. Most of the flow exits the region between core and CCP through the radial gap below porous skirt and core top. A minor portion (about 10%) exits through the porous skirt itself. This can be seen more clearly in Fig. 5 (right). Another part of core flow enters the inter-wrapper space. The amount of flow entering inter-wrapper flow is miniscule with velocities being very small when compared to the flow through the other two paths. This makes it difficult to discern from velocity vector plots. However, the effect of this flow is clearly visible in temperature contour plots in Fig. 6. In Fig. 6 temperatures at two radial planes through axis of two

IHXs are plotted. Hot sodium entering inter-wrapper space through the gap between SA outlets heats up the region below core top. This flow meets cold sodium entering this region from grid plate top (top leakage flow) and leads to a relatively sharp temperature interface on inner vessel. This sharp interface on Inner Vessel can be observed from Fig. 9 as well where temperatures on inner surface of inner vessel are plotted.

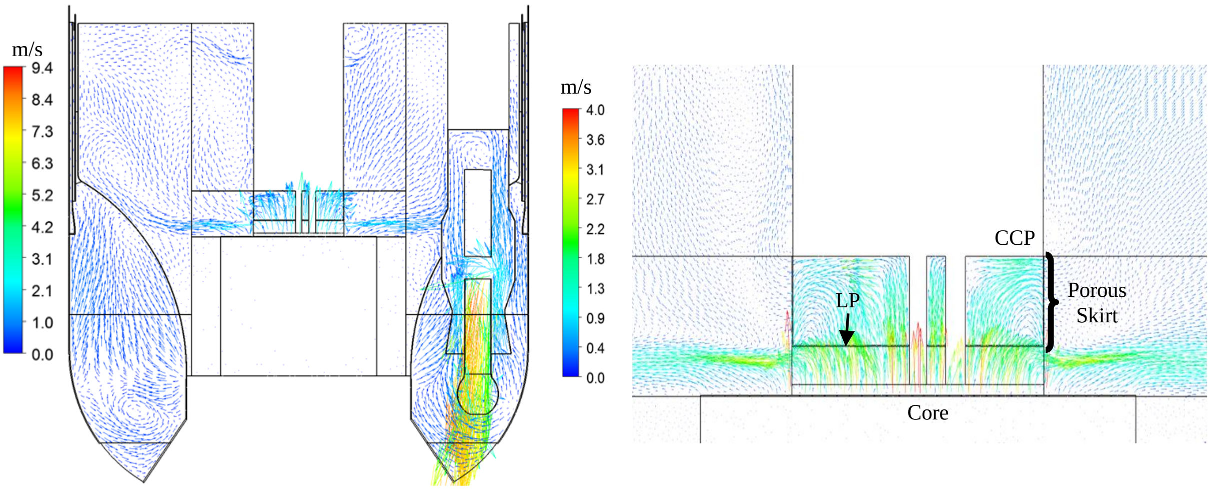

FIG. 5: Cross-sectional velocity vectors in hot and cold pools(left) with below control plug region (right)

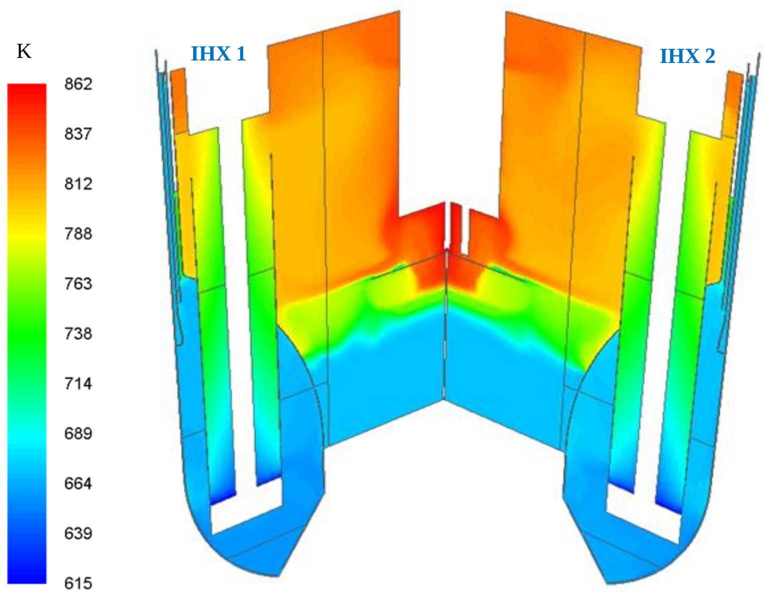

FIG. 6: Temperature contours at radial sections through IHX 1 and 2

In Fig. 7, velocity vectors at an axial section coinciding with axes of primary pipes are plotted. This section lies completely within cold pool and shows an asymmetry with respect to flow conditions persisting at outlets of the two IHXs that are part of the present model. Along the circumferential direction, IHX1 is surrounded by One PSP and one IHX (beyond symmetry plane not included in the present model).The other IHX is surrounded by two PSPs one on each side. As a result, all the flow from IHX1 has to flow towards PSP-1, while that from IHX-2 would be shared between PSP-1 and PSP-2. The velocity of flow within primary pipes ranges from 6.9 m/s to 7.2 m/s with some non- uniformity due to the asymmetric arrangement in cold pool indicated earlier. Maximum cross flow velocities of the order of 1 m/s are observed close to primary pipes. Free surface velocities for hot pool are plotted in Fig.8. Maximum velocity is of the order of 0.4 m/s which is in line with desired velocities from point of view of gas entrainment and reported earlier [4].

In Fig. 6, a few relatively pronounced temperature gradient fronts are visible. The first and the most prominent is the one on inner vessel due to the influence of inter-wrapper flow. There is another such front on PSP standpipe that can also be seen in Fig. 10. This front coincides with sodium level in PSP standpipe above which the inner surface of PSP standpipe is the argon space. Also, sodium exiting holes on lateral shell of control plug drain into relatively cooler sodium in hot pool. As a result, due to buoyancy, this sodium is pushed towards the surface. As these streams (especially from the top two rows) meet inner vessel close to free surface, its downward movement is constrained by the anti-gas entrainment baffle. As a result, there is a relatively sharper temperature variation in inner vessel across the baffle as well.

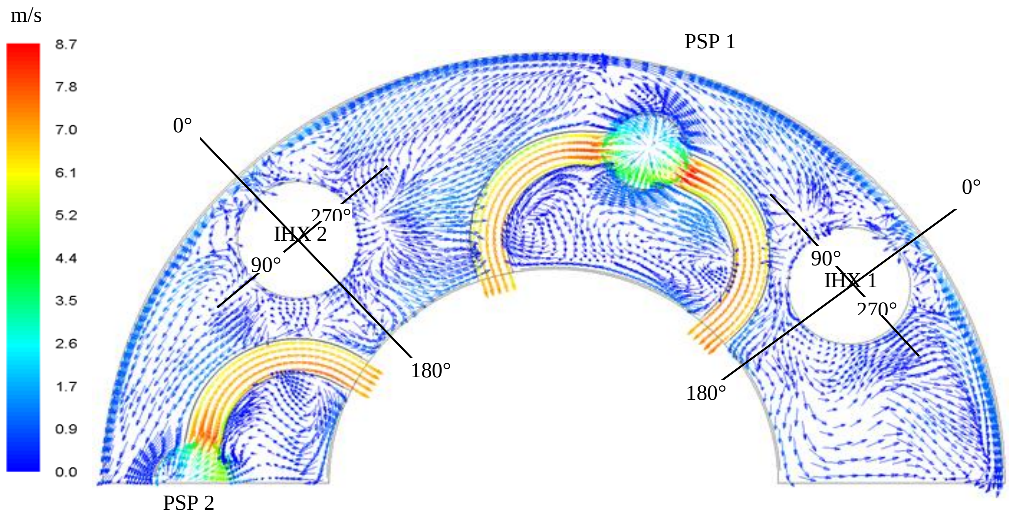

FIG. 7: Velocity vectors in an axial section (through axes of primary pipes) of cold pool

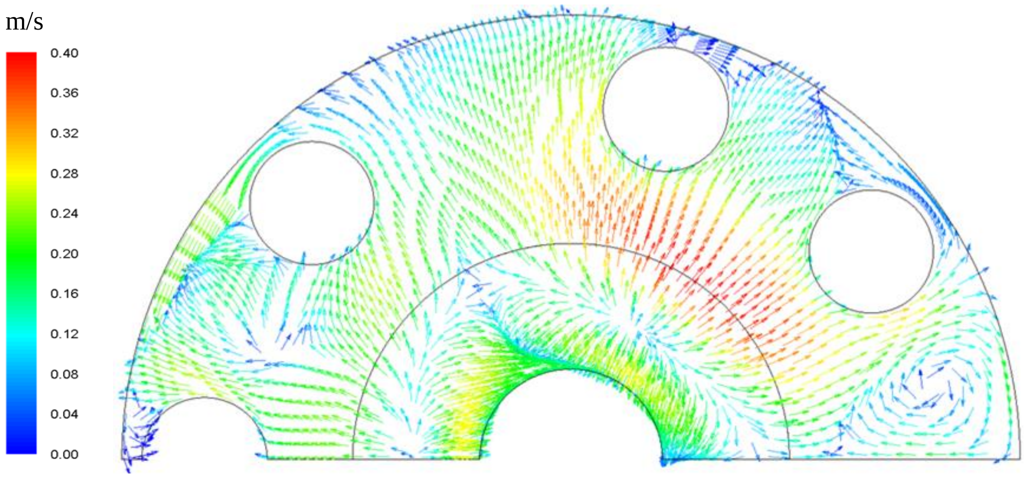

FIG. 8: Velocity vectors at free surface in hot pool

The bulk temperature of sodium entry into IHX inlet window(s) is found to be about 803 K with sodium exiting at a bulk temperature of 667 K. Heat sink inside IHX is assumed to be uniform as temperature within IHX is beyond the scope of the present study as this would require modelling of secondary side as well. However, a uniform heat sink would be expected to predict exit conditions correctly. It can be seen from Fig. 6 that the minimum temperature within IHX drops to 615 K which is substantially different from bulk exit temperature. At IHX exit window, sodium temperature is found to vary from a minimum of 620 K at the bottom of IHX window to a maximum of 690 K at top of IHX window. More detailed results are presented in a later section. Effect of this non-uniform sodium exit temperature at IHX outlet is seen on main vessel surface in Fig. 9, where the range of minimum to maximum surface temperatures becomes 649 K to 678 K. The temperature of the top half of main vessel's inner surface is uniform due to the presence of main vessel cooling system. The temperatures of various immersed parts like PSP standpipes, IHX shell, Primary piping, spherical headers etc. are shown in Fig. 10. These temperatures would be useful for thermo-mechanical analysis of these components.

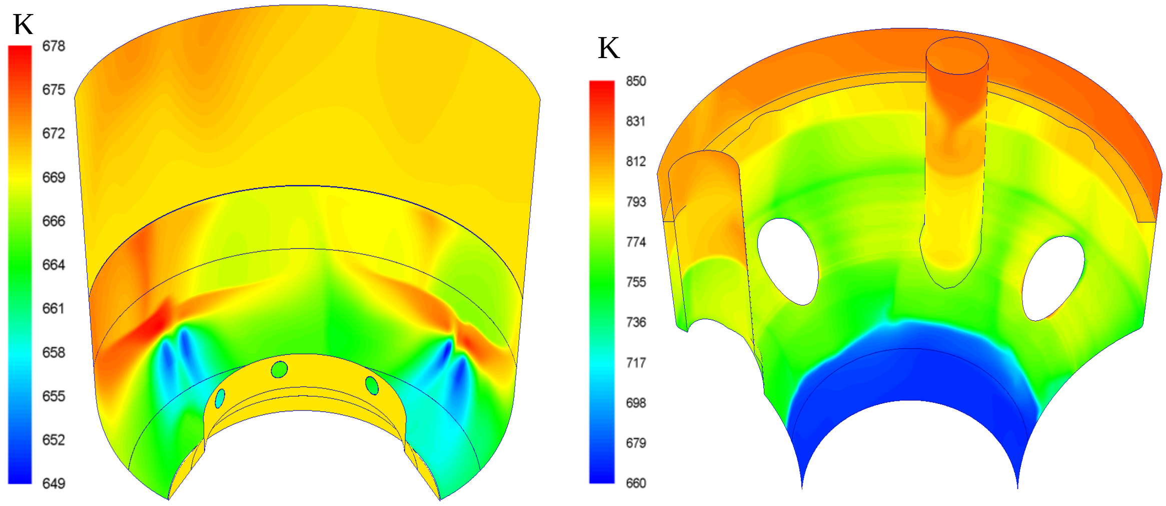

FIG. 9: Temperature contours on inner surfaces of main (left) and inner (right) vessels

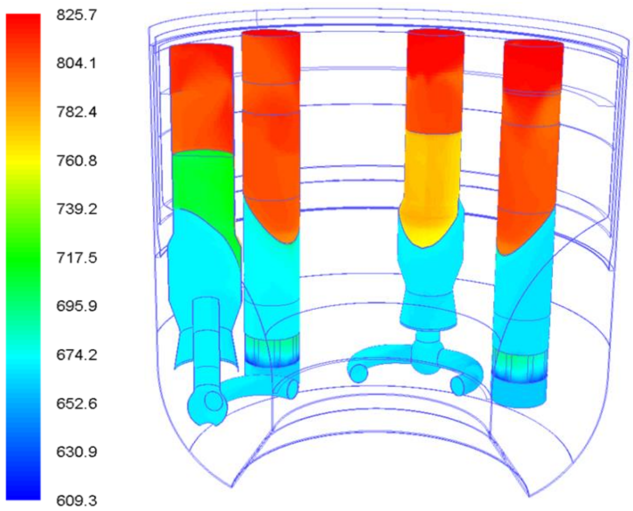

FIG. 10: Temperature contours on outer surfaces of immersed components

3.2. Inner Vessel

Axial variation of surface temperatures of inner vessel is plotted in Fig. 11 for two circumferential positions. Angles used to mark circumferential positions can be seen in Fig. 1. Elevations are measured from GP top. The total bypass heat flow from hot pool to cold pool through inner vessel is found to be 15.4 MW. The maximum temperature difference between inner and outer surfaces of inner vessel is found to be about 82 K observed for circumferential position of 105° (between PSP 1 and IHX 2). The elevation for this temperature difference is at about 4.5-5 m above GP within the toroidal redan portion.

Hot sodium from core outlet after exiting below porous skirt impacts inner vessel in this portion. As a result, inner vessel also sees the highest temperatures within this zone. Also, as can be seen in Fig. 6, the zone where GP top leakage flow (low temperature sodium) meets hot inter-wrapper sodium entering from top there is a high thermal gradient. Thermal gradient on inner and outer surfaces of inner vessel are 220 K/m and 80 K/m respectively. The other major sharp temperature gradient (indicated earlier) is at an elevation of about 8.5 m close to the position of anti-gas entrainment baffle where within a short distance of 200 mm the temperature of both surfaces of inner vessel increases by about 28 K (140 K/m). However, this does not have any implication on temperature difference across inner vessel due to this elevation being above cold pool level with the outer surface being exposed to Argon. In the present study, outer surface of inner vessel exposed to argon is an adiabatic surface. The temperature distribution on inner vessel surfaces is necessary to determine thermal loads on the component.

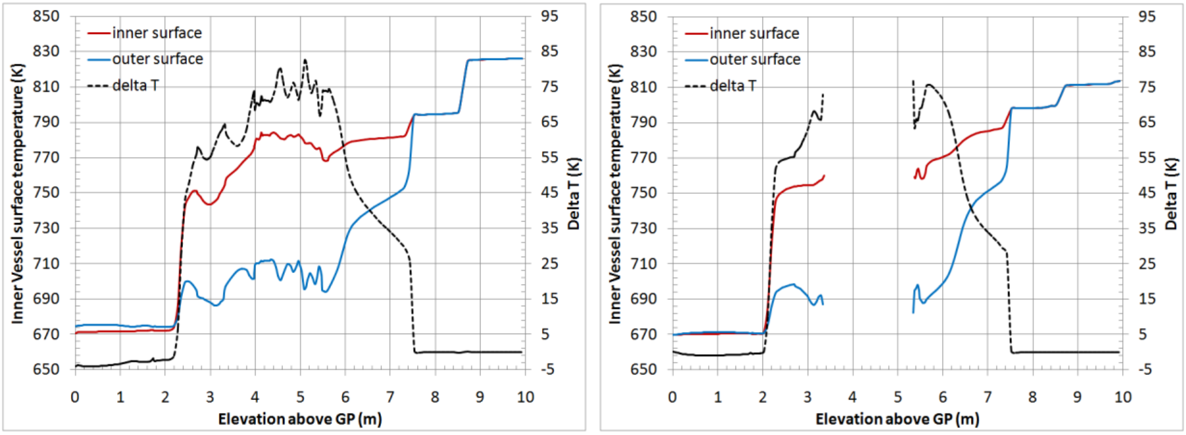

FIG. 11: Surface temperatures of IV at angular position of 0º (symmetry plane) and angular position of 180º (PSP-2 position).

3.3. Velocity and temperature profiles at IHX inlets and outlets

Radial velocities at inlet and outlet window of IHX-2 for different circumferential positions are plotted in Fig. 12. Radial velocities represent the cross flow component of velocity w.r.t. IHX tube bundle and are significant only in the window regions. These velocities can be used for the flow induced vibration studies of IHX tube bundle. The angular positions for these plots are marked in Fig. 7. Axial positions are taken from IHX window bottom. It can be seen here that radial inward superficial velocities at IHX inlet windows vary from minimum of 0.35 m/s to a maximum of 0.9 m/s. The maximum velocity is at lowest elevation along IHX window. Also, circumferential variation is minimal with similar velocity patterns seen for all circumferential positions. However, velocities are marginally higher for 0° positions.

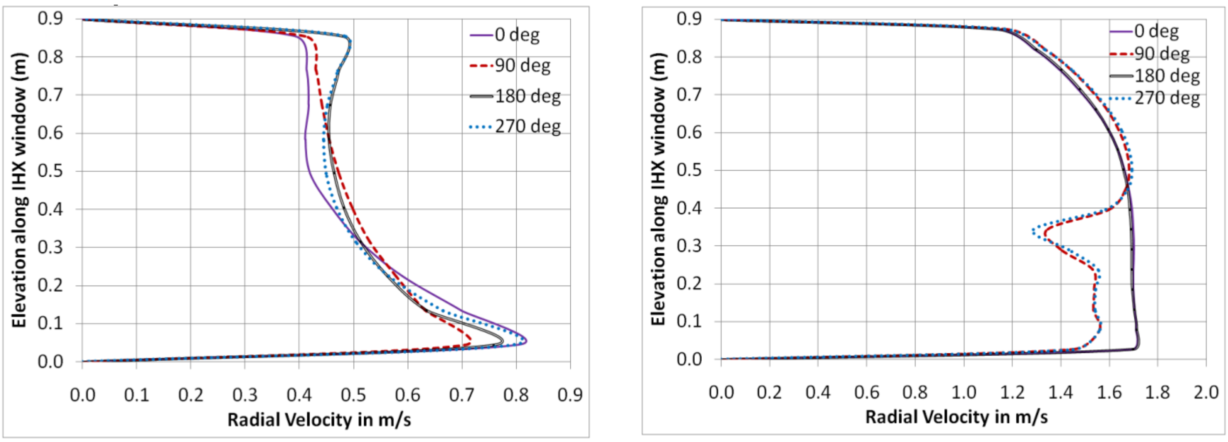

FIG. 12: Velocity distribution at inlet (left) and outlet (right) windows of IHX-2

At the outlet window, outward radial velocities vary from 1.2 m/s to 1.8 m/s. The velocities are much more uniform as compared to velocities at inlet windows. Temperature profiles for inlet and outlet windows of IHX 2 are plotted in Fig. 13. The maximum axial temperature difference for inlet window is about 20 K while that for outlet window is 60 K.

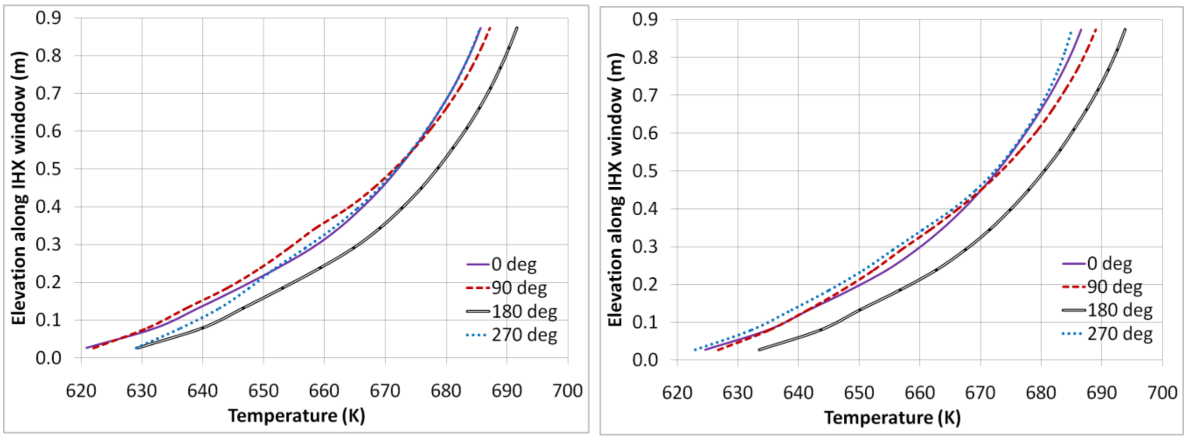

FIG. 13: Temperature distribution at inlet (left) and outlet (right) windows of IHX-2

4. CONCLUSION

An integrated thermal hydraulic analysis of cold pool and hot pool using a 180° three dimensional CFD model has been carried out. This analysis required development of an intricate model of reactor pool along with immersed components. The magnitude and diversity of geometric scales in the problem along with the requirement of resolution of temperatures in several solid structures made this a highly challenging and computationally intensive study. Important results including temperature distribution on inner vessel, main vessel, PSP standpipe, primary pipes etc. have been determined. The maximum temperature difference across inner vessel is found to be about 82 K. Heat flow through inner vessel from hot to cold pool is found to be 15.4 MW. Other important aspects predicted include (i) cross flow velocity patterns in cold pool, (ii) free surface velocity profile in hot pool (maximum velocity of 0.4 m/s) and (iii) velocity & and temperature distributions at IHX inlet and outlet windows. These results are useful in thermo-mechanical analysis of reactor assembly components.

5. ACKNOWLEDGEMENT

The authors wish to acknowledge software support from Safety Research Institute, AERB, Kalpakkam.

REFERENCES

[1] RAM KUMAR MAITY, VELUSAMY, K., SELVARAJ, P., CHELLAPANDI, P., “Integrated pool thermal hydraulics of a Fast Breeder Reactor – Inner vessel temperature distribution”, 22th National and 11th International ISHMT-ASME Heat and Mass Transfer Conference (Proc. Int. Conf., IIT Kharagpur, India, 2013), IIT KGP, Kharagpur (2013), Paper HMTC1300433.

[2] ABHITAB BACHCHAN, DEVAN K., PUTHIYAVINAYAGAM P., SRINIVASAN G., “Conceptual Design of Future Fast Reactor Core with Enhanced Safety and High Breeding”, 20th National Symposium on Radiation Physics (Proc. NSRP 20, India, 2013), CARER, Mangalore (2015).

[3] VELUSAMY K., et. al., Primary system thermal hydraulics of future Indian fast reactors, Nuclear Engg. & Design, 294 (2015) 170-182.

[4] BANERJEE, I., et. al., Development of gas entrainment mitigation devices for PFBR hot pool, Nuclear Engg. & Design, Vol.258 (2013) 258-265.

[5] WARDSMITH, A J., Pressure Losses in Ducted Flows, Butterworths, London (1971)

[6] ZUKAUSKAS A., ULINSKAS R.,, Banks of plain and finned tubes, Heat Exchanger Design Handbook, Hemisphere Publishing Corporation, 1983

[7] KUNDU, P K., COHEN, I M., DOWLING, D R., Fluid Mechanics – Fifth Ed., Academic Press, Oxford, 2012

[8] ANSYS, INC., Ansys FLUENT-V 19.2, Theory Guide.